

Entanglement-variational Hardware-efficient Ansatz for Eigensolvers

Xin Wang,^{1,2} Bo Qi,^{1,2,*} Yabo Wang,^{1,2} and Daoyi Dong³

¹*Key Laboratory of Systems and Control, Academy of Mathematics and Systems Science,
Chinese Academy of Sciences, Beijing 100190, P. R. China*

²*University of Chinese Academy of Sciences, Beijing 100049, P. R. China*

³*CIICADA Lab, School of Engineering, Australian National University, Canberra ACT 2601, Australia*

(Dated: March 18, 2024)

Variational quantum eigensolvers (VQEs) are one of the most important and effective applications of quantum computing, especially in the current noisy intermediate-scale quantum (NISQ) era. There are mainly two ways for VQEs: problem-agnostic and problem-specific. For problem-agnostic methods, they often suffer from trainability issues. For problem-specific methods, their performance usually relies upon choices of initial reference states which are often hard to determine. In this paper, we propose an Entanglement-variational Hardware-efficient Ansatz (EHA), and numerically compare it with some widely used ansatzes by solving benchmark problems in quantum many-body systems and quantum chemistry. Our EHA is problem-agnostic and hardware-efficient, especially suitable for NISQ devices and having potential for wide applications. EHA can achieve a higher level of accuracy in finding ground states and their energies in most cases even compared with problem-specific methods. The performance of EHA is robust to choices of initial states and parameters initialization and it has the ability to quickly adjust the entanglement to the required amount, which is also the fundamental reason for its superiority.

I. Introduction

Quantum computing has the potential to revolutionize many fields, including quantum many-body physics [1–3], quantum chemistry [4–6], material science [7–9], and so on [10, 11]. Among these, finding ground states and their corresponding energies of Hamiltonians is a fundamental problem [1–5]. In the current noisy intermediate-scale quantum (NISQ) era [12–14], variational quantum eigensolvers (VQEs) [15–19] have been proposed to solve this problem with the hope that approximate solutions could be found for large systems which are intractable with classical computers.

VQEs work in a hybrid quantum-classical manner [20]. They employ a parameterized quantum circuit (PQC) to generate parameterized trial states and the variational parameters are updated by a classical optimizer through minimizing the objective function, which in general is the expectation value of the Hamiltonian with respect to the trial state.

To enhance performance of VQEs, various methods have been developed from different perspectives. These include designing appropriate ansatzes for quantum circuits [21–27], tailored initial states [28, 29], proper parameter initializations [30, 31], developing efficient optimization methods [32], employing feedback for iterations [33], and utilizing classical post-processing with neural networks [34], among others [35–37]. It is clear that the ansatz of a quantum circuit directly determines the success of VQEs. For instance, if the quantum circuit is poorly expressible that cannot generate trial states close to the target state, then no other auxiliary methods can improve its performance [38, 39]. There are

mainly two ways to design ansatzes for quantum circuits: problem-agnostic and problem-specific [16].

Hardware-efficient ansatz (HEA) is a well-known and widely used problem-agnostic method, which seeks to minimize the hardware noise by using native gates and connectives [40–42]. When training quantum circuits based on HEAs, it often faces many challenges. Shallow HEA circuits are poorly expressible, and may cause the landscape of the cost function to be swamped with spurious local minima under global measurements [43, 44]. Deep circuits, however, will make the PQC too expressive resulting in barren plateaus (BPs) [45, 46], i.e., the cost gradient is exponentially small with the number of qubits and/or the circuit depth. Both of these issues will make the PQC training extremely difficult. A major reason is that in most of existing HEAs, the entanglers are usually fixed, resulting in a lack of freedom to quickly adjust the entanglement of the trial states to the required amount. It is clear that the nature of the circuit ansatz determines the level of entanglement that can be achieved. On the one hand, generating a matched amount of entanglement is necessary to guarantee the convergence of eigensolvers based on HEAs. On the other hand, while entanglement can usually be quickly generated within a few layers, the excess entanglement cannot be removed efficiently [47]. It has been pointed out in [48] that if the generated entanglement does not match the problem under study, it may hamper the convergence process. Moreover, it was argued in [49] that too much entanglement can result in BPs. In addition, it was stated in [50] that even for shallow circuits, entanglement satisfying volume law should be avoided.

To address the training issues of PQCs, it has been suggested to design circuit ansatzes in a problem-specific manner. Examples include the Hamiltonian variational ansatz (HVA) also commonly referred to as a Trotterized

* qibo@amss.ac.cn

adiabatic state preparation ansatz [51], and the hardware symmetry preserving ansatz proposed in [52], which reduces the explored space of unitaries through symmetry preserving and is referred to as HSA in our paper. In quantum computational chemistry, some chemically inspired ansatzes have been proposed by adapting classical chemistry algorithms to run efficiently on quantum circuits [4]. The most notable one is the unitary coupled cluster (UCC) [53] adapted from the coupled cluster (CC) method [54]. The variational UCC method is able to converge when used with multi-reference initial states. The UCC is usually truncated at the single and double excitations, known as UCCSD [53]. In similar spirit to UCCSD, another commonly used ansatz has been proposed in [55], which considers all single and double excitation gates acting on the reference state without flipping the spin of the excited particles, but where all gates are Givens rotations [55]. We refer to this ansatz as Givens rotation with all singles and doubles (GRSD) in this paper. Moreover, adaptive ansatzes have been presented in [22, 23, 56], where the structure of quantum circuits are optimized adaptively. It has been shown that these adaptive ansatzes perform better in terms of both circuit depth and chemical accuracy than circuits that use parameters update alone. For these problem-specific methods, their performance usually relies upon choices of initial reference states [57–59], which are often hard to determine.

In this paper, we present a hardware-efficient ansatz for eigensolvers which allows for rapid adjustment of the entanglement to the required amount by making entanglers variational. Our ansatz is thus referred to as Entanglement-variational Hardware-efficient Ansatz (EHA). We validate its efficiency via numerical comparisons with some widely used VQE ansatzes. By solving benchmark problems in quantum many-body physics and quantum chemistry, our EHA has the following advantages: 1) It is hardware-efficient and can be applied to various kinds of problems, particularly suitable for NISQ devices. 2) In most of numerical experiments, EHA can attain a higher level of accuracy than other ansatzes, even as compared with problem-specific ansatzes. 3) For different choices of initial reference states and variational parameters, the performance of EHA is more robust as compared to other ansatzes. 4) The variational entangler design enables EHA to quickly adjust the entanglement to the desired amount, which is also the fundamental reason for its superiority.

This paper is organized as follows. In Section II, for subsequent comparison, we first introduce several basic models and corresponding ansatzes. Then we present our EHA, and demonstrate its advantages via numerical comparisons with other ansatzes in Section III. Section IV concludes the paper. Since we utilize many abbreviations, for the convenience of reading, we summarize the frequently-used abbreviations and their full expressions in Table I.

Abbreviations	Descriptions
Quantum many-body model	
HM	Heisenberg Model
TFIM	Transverse Field Ising Model
BHM	Bose Hubbard Model
Variational Quantum Eigensolver(VQE) ansatz	
EHA	Entanglement-variational Hardware-efficient Ansatz
HEA	Hardware-Efficient Ansatz
HVA	Hamiltonian Variational Ansatz
HSA	Hardware Symmetry preserving Ansatz
GRSD	Givens Rotations with all Single and Double excitations
UCCSD	Unitary Coupled Cluster with all Single and Double excitations
ADAPT-VQE	Adaptive Derivative-Assembled Pseudo-Trotter ansatz-VQE

TABLE I. Glossary.

II. Preliminaries

In this paper, we focus on the task of finding ground eigenstates and their corresponding eigenenergies of Hamiltonians in quantum many-body physics and quantum chemistry. In this section, we introduce the models and ansatzes to be used for comparison with our EHA.

A. Quantum many-body models

For quantum many-body physics, we first consider a 1-dimensional chain Heisenberg model (HM) consisting of N spins [51, 52], whose Hamiltonian reads

$$H_{\text{HM}} = J \sum_{i=1}^{N-1} (\sigma_i^x \sigma_{i+1}^x + \sigma_i^y \sigma_{i+1}^y + \sigma_i^z \sigma_{i+1}^z), \quad (1)$$

where $J = 1$ sets the unit of energy, σ_i^x , σ_i^y and σ_i^z denote the Pauli X , Y and Z operators acting on the i -th qubit, respectively. The Hamiltonian Eq. (1) describes a model of interacting systems that cannot be mapped to free fermions. It supports symmetries including the conservation of the spin components in all directions, i.e., $[H_{\text{HM}}, S_\alpha] = 0$ with $S_\alpha = \frac{1}{2} \sum_i \sigma_i^\alpha$ for $\alpha = x, y$ and z , as well as the total spin, namely $[H_{\text{HM}}, S_{\text{tot}}^2] = 0$ with $S_{\text{tot}}^2 = S_x^2 + S_y^2 + S_z^2$.

We also consider free fermionic systems described by the transverse field Ising model (TFIM) [51, 52], whose Hamiltonian reads

$$H_{\text{TFIM}} = J_z \sum_{i=1}^{N-1} \sigma_i^z \sigma_{i+1}^z + h_x \sum_{i=1}^N \sigma_i^x, \quad (2)$$

where J_z represents the exchange coupling and h_x depicts the strength of the transverse magnetic field. For this Hamiltonian, it is well-known that a quantum phase

transition occurs at $J_z = h_x$, and at this critical point, the ground state is highly entangled and in a complex form [52].

B. Hardware-efficient ansatzes

In the NISQ era, VQEs have been proposed for eigensolvers with the hope to demonstrate potential quantum advantages when dealing with large systems which are beyond the power of classical computers.

Given a Hamiltonian H , when employing VQEs, we first need to design an ansatz to build a PQC $U(\theta)$ with variational parameters θ . Starting from a given initial reference state $|\psi_0\rangle$, we use the generated trial state $|\psi(\theta)\rangle = U(\theta)|\psi_0\rangle$ to approximate the ground state of H . The variational parameters θ are adaptively updated by a classical optimizer via minimizing the expectation of H at the trial state, which reads

$$C(\theta) = \text{Tr} [HU(\theta)|\psi_0\rangle\langle\psi_0|U^\dagger(\theta)]. \quad (3)$$

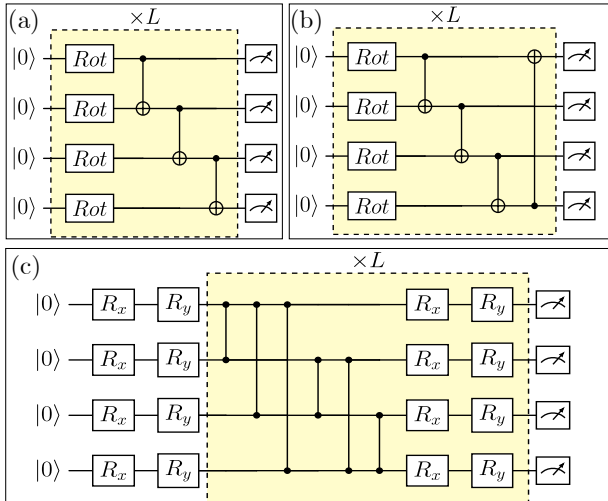


FIG. 1. Quantum circuits for HEAs. (a) CX-line, whose single-qubit modules are *Rot* gates defined in Eq. (4), and the entangling gates are CX gates arranged in a line pattern. (b) CX-ring, whose entangling gates are arranged in a ring pattern. (c) CZ-complete, whose single-qubit modules are $R_y R_x$ gates, and the entangling gates are CZ gates arranged in a complete pattern. The yellow shaded circuits are repeated for L times.

To minimize the hardware noise in the NISQ era, HEAs have been widely used for eigensolvers. Three commonly used HEAs are illustrated in Fig. 1, and will be compared with our EHA. The initial reference state of these three HEAs is usually set to be $\rho_0 = |0\rangle\langle 0|$. For the circuit in Fig. 1(a), the single-qubit rotations take the form of

$$\text{Rot}(\phi, \theta, \omega) = R_z(\omega)R_y(\theta)R_x(\phi), \quad (4)$$

with $R_z(\phi) = e^{-i\phi Z/2}$, $R_y(\theta) = e^{-i\theta Y/2}$, and the entangling gates are CX gates arranged in a line pattern [42].

Thus, we refer to it as CX-line. The ansatz in Fig. 1(b) is named after CX-ring, since its single-qubit modules and entangling gates are the same as those in CX-line, except that the entangling gates are in a ring pattern [41]. For the ansatz in Fig. 1(c), its single-qubit rotations are in the form of $R_y(\theta)R_x(\phi)$ with $R_x(\phi) = e^{-i\phi X/2}$ [31]. Since its entangling gates are CZ gates arranged in a complete pattern [60], we call it CZ-complete.

C. Problem-specific ansatzes

The problem-agnostic HEAs often suffer from difficult training issues. In addition, HEAs do not preserve any symmetry in general. In this subsection, we briefly introduce two important problem-specific ansatzes: Hamiltonian variational ansatz (HVA) [51] and hardware symmetry preserving ansatz (HSA) [52].

HVA: Assume the Hamiltonian H can be decomposed into a summation with a total number of S terms as

$$H = \sum_{s=1}^S H_s. \quad (5)$$

Then we can construct the HVA in the form of

$$U(\theta) = \prod_{l=1}^L \left[\prod_{s=1}^S \exp(-i\theta_{l,s} H_s) \right]. \quad (6)$$

Specifically, for an N -qubit HM described by Eq. (1), when the qubit number is even, its Hamiltonian can be decomposed into [51]

$$H_{\text{HM}} = H^{\text{even}} + H^{\text{odd}},$$

with

$$\begin{aligned} H^{\text{even}} &= H_{xx}^{\text{even}} + H_{yy}^{\text{even}} + H_{zz}^{\text{even}}, \\ H^{\text{odd}} &= H_{xx}^{\text{odd}} + H_{yy}^{\text{odd}} + H_{zz}^{\text{odd}}, \end{aligned}$$

where for $\alpha = x, y$ and z , $H_{\alpha\alpha}^{\text{even}} = \sum_{i=1}^{N/2} \sigma_{2i-1}^\alpha \sigma_{2i}^\alpha$ and $H_{\alpha\alpha}^{\text{odd}} = \sum_{i=1}^{N/2-1} \sigma_{2i}^\alpha \sigma_{2i+1}^\alpha$. Then $U_{\text{HM}}(\theta, \phi, \beta, \gamma)$ reads

$$\begin{aligned} U_{\text{HM}}(\theta, \phi, \beta, \gamma) &= \prod_{l=1}^L \left[G(\gamma_l, H_{xx}^{\text{even}}) G(\gamma_l, H_{yy}^{\text{even}}) \right. \\ &\quad \left. G(\beta_l, H_{zz}^{\text{even}}) G(\phi_l, H_{xx}^{\text{odd}}) G(\phi_l, H_{yy}^{\text{odd}}) G(\theta_l, H_{zz}^{\text{odd}}) \right], \end{aligned}$$

with $G(x, A) = e^{-i\frac{x}{2}A}$.

The whole circuit for $U_{\text{HM}}(\theta, \phi, \beta, \gamma)$ can be found in Fig. 19 in Appendix A. To implement $U_{\text{HM}}(\theta, \phi, \beta, \gamma)$, the entangling operators, $XX(\phi) = e^{-i\frac{\phi}{2}(X \otimes X)}$, $YY(\phi) = e^{-i\frac{\phi}{2}(Y \otimes Y)}$ and $ZZ(\phi) = e^{-i\frac{\phi}{2}(Z \otimes Z)}$, are employed whose circuits are illustrated in Fig. 2.

Note that the initial reference state plays a crucial role in problem-inspired ansatzes [28, 29], which is quite different from the case in HEAs. To guarantee the efficiency

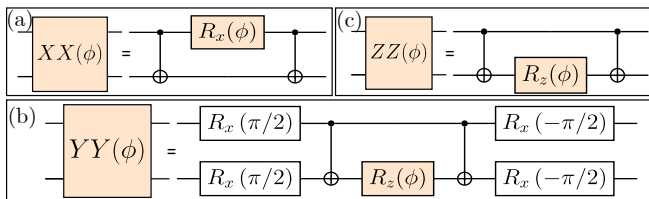


FIG. 2. Hardware-efficient circuits for entangling gates. (a) Circuit for XX . (b) Circuit for YY . (c) Circuit for ZZ .

of HVA for HM, the initial reference state is chosen to be $\otimes^{\frac{N}{2}} |\Psi^-\rangle$ with $|\Psi^-\rangle = \frac{1}{\sqrt{2}}(|01\rangle - |10\rangle)$.

As for an N -qubit TFIM with $J_z = h_x = -1$ and N being even, the Hamiltonian H_{TFIM} can be decomposed into

$$H_{\text{TFIM}} = - \sum_{i=1}^{N-1} \sigma_i^z \sigma_{i+1}^z - \sum_{i=1}^N \sigma_i^x = H_{zz} + H_x, \quad (7)$$

with $H_{zz} = - \sum_i \sigma_i^z \sigma_{i+1}^z$ and $H_x = - \sum_i \sigma_i^x$. Then the HVA $U_{\text{TFIM}}(\boldsymbol{\beta}, \boldsymbol{\gamma})$ reads

$$U_{\text{TFIM}}(\boldsymbol{\beta}, \boldsymbol{\gamma}) = \prod_{l=1}^L \left[\exp(-i \frac{\gamma_l}{2} H_x) \exp(-i \frac{\beta_l}{2} H_{zz}) \right],$$

whose circuit diagram is illustrated in Fig. 21(a) in Appendix A. For TFIM, the initial reference state is chosen to be $\otimes^N |+\rangle$ with $|+\rangle = \frac{1}{\sqrt{2}}(|0\rangle + |1\rangle)$.

HSA: In [52], a HSA was proposed to improve the performance of eigensolvers by exploiting the symmetries of the Hamiltonian.

To be specific, if the ansatz $U(\boldsymbol{\theta})$ satisfies $[U(\boldsymbol{\theta}), S_z] = 0$, then it conserves the number of excitation. While if $[U(\boldsymbol{\theta}), S_{\text{tot}}^2] = 0$, then it preserves the total spin. To realize HSA, the following more complex entangling gate [61]

$$\mathcal{N}(\theta, \phi, \beta) = e^{i(\theta \sigma_1^x \sigma_2^x + \phi \sigma_1^y \sigma_2^y + \beta \sigma_1^z \sigma_2^z)}.$$

has been employed. The circuit of realizing $\mathcal{N}(\theta, \phi, \beta)$ is shown in Fig. 1(b) in [52] (Fig. 20(b) in Appendix A).

As for the HM in Eq. (1), a single block circuit for realizing S_z -conserving and S_{tot} -conserving ansatz is shown in Fig. 1(c) and Fig. 1(d) in [52], respectively. For ease of reading, we illustrate the HSA circuit in Fig. 20 in Appendix A. Since the ground state of the Hamiltonian Eq. (1) is a global singlet with both the total spin $s = 0$ and the spin component $s_z = 0$, the initial reference state is chosen to be $\otimes^{\frac{N}{2}} |\Psi^-\rangle$ to guarantee the preservation of these symmetries in trial states.

The authors in [52] also generalized HSA to solve TFIM, whose circuit is shown in Fig. 7(a) in [52] (Fig. 21(b) in Appendix A). The initial reference state is chosen to be $\otimes^N |+\rangle$.

D. Quantum chemistry models and ansatzes

Solving the low lying energies of the electrons in molecules has attracted significant attention [4] since it was first introduced by [62] in the context of quantum computational chemistry. It is often a starting point for more complex reaction analysis in chemistry, including the calculation of reaction rates, the determination of molecular geometries and thermodynamic phases, among others [63].

In this paper, we try to find the ground eigenstates and eigenenergies of the electronic Hamiltonian of H_3^+ cation, HF, H_5 , BeH_2 and LiH molecules. For conciseness, we work in atomic units, where the length unit is 1 Å (1 Å = 1×10^{-10} m), and the energy unit is 1 Hartree (1 Hartree = 27.211 eV). We utilize the second quantized representation to simulate chemical systems on a quantum computer [64]. To do this, we need to select a basis set, which is used to approximate the spin-orbitals of the investigated molecule. A suitably large basis set is crucial for obtaining accurate results. In this paper, we take the Slater type orbital-3 Gaussians (STO-3G) [65] as the spin-orbital basis for second quantization. Then we utilize the occupation number basis to represent whether a spin-orbital is occupied. Next we can employ the Jordan-Wigner encoding [66] to map the second quantized fermionic Hamiltonian into a linear combination of Pauli strings, each of which is a product of single qubit Pauli operators. More details can be found in [4].

While it is important to understand the whole procedure of how to map electronic structure problems onto a quantum computer, every step from selecting a basis to producing an encoded qubit Hamiltonian can be carried out using a quantum computational chemistry package such as OpenFermion [67] and PennyLane [68]. In this paper, we adopt PennyLane to implement UCCSD and GRSD.

III. Main Results

In this section, we first present our hardware-efficient ansatz having variational entangling gates for eigensolvers. We then compare it with the ansatzes introduced by focusing on models introduced in Section II.

A. Entanglement-variational hardware-efficient ansatz

Our aim is to design a hardware-efficient ansatz for eigensolvers which can be efficiently applied to solve various kinds of Hamiltonians for different systems.

To approximate target ground states, it is imperative to generate trial states having a matched amount of entanglement. However, there is a lack of freedom to adjust entanglement to the required level in most of exist-

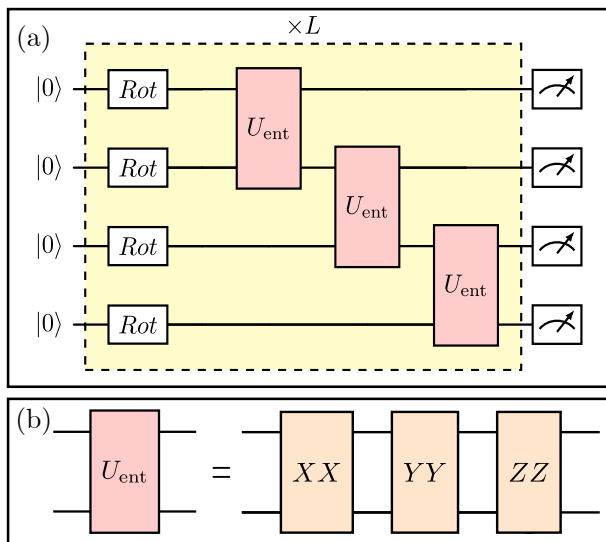


FIG. 3. Quantum circuit for EHA. (a) The circuit consists of L blocks, and each block is composed of a layer of single qubit rotational gates defined by Eq. (4) and variational entanglers U_{ent} arranged in a line pattern. (b) Each variational entangler U_{ent} is composed of XX , YY and ZZ gates in series, whose realizations are illustrated in Fig. 2. The variational parameters of the entanglers are (in general) different. The initial reference state is set to be $\otimes^n |0\rangle$.

ing HEAs, as their entanglers are fixed. The entanglement can usually be generated within a few layers, however, once the entanglement is in excess of requirement, it cannot be removed efficiently. The excess entanglement will result in too much expressibility leading to the phenomenon of BPs, which makes the training extremely difficult and greatly hampers the efficiency of HEAs.

Note that the entanglement is generated through entangling gates. Therefore, to improve the ability of regulating the generated entanglement of HEAs, a natural idea is to make entangling gates tunable with variational parameters. Based on this, we present our entanglement-variational hardware-efficient ansatz (EHA) as illustrated in Fig. 3.

It is clear that the entanglers

$$U_{\text{ent}}(\boldsymbol{\theta}_{l,i}) = ZZ(\theta_{l,i,3})YY(\theta_{l,i,2})XX(\theta_{l,i,1})$$

are tunable, which is the most significant difference from existing HEAs. Our ansatz is hardware-efficient, since the variational XX , YY and ZZ gates can be realized by native single qubit gates and CX gates as illustrated in Fig. 2. Moreover, we would like to point out that since the entanglers XX , YY and ZZ are native to hardware themselves in some quantum computers [69], this can further significantly improve the efficiency of our EHA.

Although HVA and HSA also employ variational XX , YY and ZZ gates to implement entangling operations, the principle of their design is rather different from our EHA. There they first decompose the Hamiltonian of a specific problem into components as in Eq. (5), and

then design variational circuits to realize each component Hamiltonian as described by Eq. (6). Note that in quantum many-body physics, Hamiltonians are described in terms of Pauli strings. Thus, when realizing the component Hamiltonians, variational gates, e.g., XX , naturally appear. Their constructed circuits are problem-specific. However, our EHA is problem-agnostic and can be applied to various problems. Moreover, it is worth pointing out that for the HM, although the circuits of EHA (Fig. 3), HVA (Fig. 19) and HSA (Fig. 20) appear similar apart from the way the entangling gates are arranged, there is an additional layer of single-qubit rotational gates with each having three variational parameters as described by Eq. (4) for each block. For the TFIM, compared to HVA and HSA (Fig. 21), each block of EHA (Fig. 3) has more degrees of freedom in adjusting the entangling and single-qubit variational gates. It has been demonstrated in [70] that by increasing the number of variational parameters, local minima of the cost function can be transformed into saddle points. Furthermore, it has been shown that gradient descent only converges to minima rather than saddle points [71]. Thus, the additional degrees of variational parameters in our EHA can help enhance the performance of eigensolvers compared to HVA and HSA. This will be validated in the following subsections.

We now compare our EHA with the ansatzes introduced in Section II in finding the ground states and their energies of Hamiltonians of various kinds of systems. In this paper, the actual ground states and their energies of Hamiltonians are obtained by employing the classical method NumPy [72]. We demonstrate that as compared with other ansatzes, our EHA can approximate the target ground states with a higher level of accuracy in most cases, and its performance is more robust with respect to different initializations and different initial reference states. In addition, our EHA can quickly adjust the entanglement of trial states to the required amount.

B. Higher level of accuracy and robustness

1. Quantum many-body problems

In the first part of Subsection III B, we focus on finding eigenstates of a 12-qubit HM in Eq. (1) and an 12-qubit TFIM in Eq. (2).

Since 2-qubit entangling gates are valuable resources in quantum computing, when comparing the performance of different ansatzes, to be fair, we ensure that they employ roughly the same number of basic 2-qubit entangling gates. As an illustration, when solving an N -qubit HM (N is even), as shown in Fig. 2 and Fig. 3, our EHA utilizes a total number of $6(N-1)$ CX gates per block. While for each block, there are $(N-1)$ CX gates for CX-line, N CX gates for CX-ring, $\frac{N(N-1)}{2}$ CZ gates for CZ-complete, $6(N-1)$ CX gates for HVA, and $3(N-1)$ CX gates for HSA. Here, we do not include the CX gates uti-

lized to prepare the initial reference states for HVA and HSA. Thus, if there are L blocks in our EHA, then the number of blocks should be $6L$ for CX-line, $\lceil \frac{6L(N-1)}{N} \rceil$ for CX-ring, $\lceil \frac{12L}{N} \rceil$ for CZ-complete, L for HVA and $2L$ for HSA. Here, $\lceil \cdot \rceil$ denotes the roundup function.

As for the initialization of variational parameters, for CZ-complete, we use Gaussian initialization whose mean is 0 and variance is $1/L$ as mentioned in [31]. While for the other ansatzes, we adopt the uniform distribution $\mathcal{U}[-\pi, \pi]$. We employ the Adam optimizer provided by PennyLane for training, and the step size is set to be 0.01 for all ansatzes, unless otherwise stated. Each ansatz is implemented 10 times, and for each realization the initial parameters are drawn according to the assumed distribution. In the following figures, otherwise stated, the black dashed line denotes the actual ground state energy of the considered case, which serves as a baseline for comparison. All the other lines indicate the respective average value of the expectation of the considered Hamiltonian over 10 realizations for different ansatzes. The shaded areas represent the smallest area that includes all the behaviors of the 10 realizations. Here, for simplicity, we do not take into account of the impact of limited measurement shots, which is a limiting factor for NISQ devices. We also perform additional experiments under limited shot counts, and the results demonstrate that our EHA has similar advantages to the ideal case (infinite shots) compared to other ansatzes. We illustrate one of the results in Appendix B.

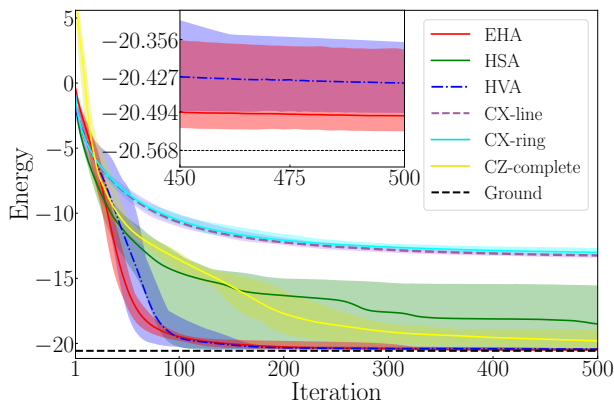


FIG. 4. Comparison of our EHA with other ansatzes for HM in Eq. (8). The inset illustrates the fine difference between EHA and HVA. Our EHA is superior to other ansatzes in obtaining a lower energy, and its performance is robust with respect to different realizations.

To compare, we first consider a 12-qubit HM, whose Hamiltonian reads

$$H_{\text{HM}} = \sum_{i=1}^N (\sigma_i^x \sigma_{i+1}^x + \sigma_i^y \sigma_{i+1}^y + \sigma_i^z \sigma_{i+1}^z), \quad (8)$$

with $N = 12$. The numbers of blocks in our EHA, CX-line, CX-ring, CZ-complete, HVA and HSA are 10, 60,

55, 10, 10 and 20, respectively. We illustrate their performance in Fig. 4. From the perspective of the average energy over different realizations, it is clear that our EHA outperforms all the other ansatzes. Among them, the performances of CX-ring and CX-line are very poor. The performance of HSA has an obvious gap with our EHA. In addition, our EHA is robust to different parameter initializations, since all the 10 realizations approximately converge to the actual ground state energy. In contrast, the performance of HSA is very sensitive to parameter initializations.

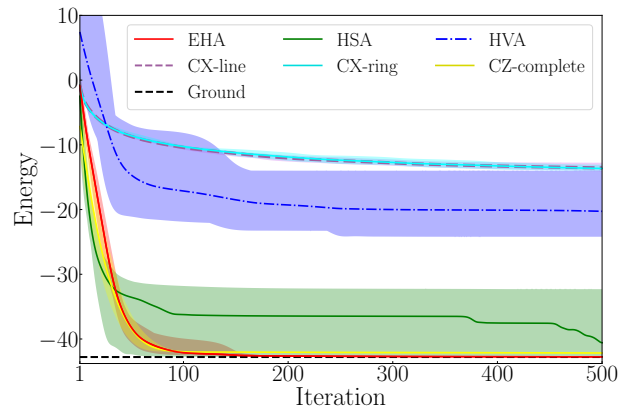


FIG. 5. Comparison of our EHA with other ansatzes for the TFIM in Eq. (9). Our EHA is much better than the other ansatzes, as it can robustly obtain a lower energy.

Next, for the 12-qubit TFIM, we first consider a Hamiltonian which reads

$$H_{\text{TFIM1}} = - \sum_{i=1}^{N-1} \sigma_i^z \sigma_{i+1}^z + 3.5 \sum_{i=1}^N \sigma_i^x, \quad (9)$$

with $N = 12$. The numbers of blocks in our EHA, CX-line, CX-ring, CZ-complete, HVA, and HSA are 4, 24, 22, 4, 4 and 8, respectively. The results are illustrated in Fig. 5. We find that our EHA outperforms all the other ansatzes, as it can robustly attain a lower energy.

Recall that HSA is a problem-specific ansatz that is utilized to improve the performance of VQE. However, from Fig. 4 and Fig. 5, it is clear that the sample variance of HSA is much larger than other ansatzes. This implies that its performance relies on different initial parameters. In fact, in the above experiments, it does not always provide a good approximation to the actual solution. However, it does converge to the solution approximately under some initializations. This is demonstrated in Fig. 6, where we plot the best performance of our EHA and HSA among 10 experiments for the HM in Eq. (8) and TFIM in Eq. (9). We find that from the perspective of the best performance, the problem-specific HSA is slightly better than our EHA. Nevertheless, it is important to note that our ansatz is problem-agnostic, and it is more robust to different realizations.

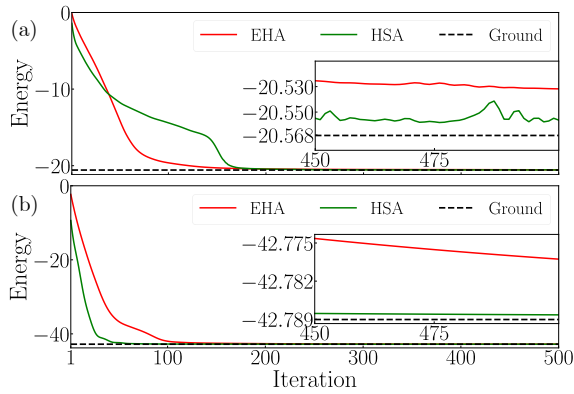


FIG. 6. The best performance of EHA and HSA among 10 experiments for (a) HM in Eq. (8) and (b) TFIM in Eq. (9). The insets illustrate their fine differences. HSA is slightly better than our EHA in obtaining a lower energy.

We then consider the TFIM in Eq. (2) with $J_z = h_x = -1$, whose Hamiltonian reads

$$H_{\text{TFIM2}} = -\sum_{i=1}^{11} \sigma_i^z \sigma_{i+1}^z - \sum_{i=1}^{12} \sigma_i^x. \quad (10)$$

Recall that for the Hamiltonian Eq. (2), a quantum phase transition occurs at $J_z = h_x$, and at this critical point, the ground state is highly entangled and in a complex form [52]. We compare our 10 blocks EHA and 20 blocks HSA, and demonstrate the experimental results in Fig. 7. We find that for the TFIM in Eq. (10), HSA converges to the actual ground state energy closer and faster than our EHA when using a step size of 0.01. To accelerate the convergence rate of EHA, we can increase its step size to 0.05 for the first 500 iterations and keep 0.01 for the rest. The accelerated version of EHA is referred to as EHA-acc. and its experimental results are also demonstrated in Fig. 7. We find that the performance of EHA-acc. is similar to that of HSA.

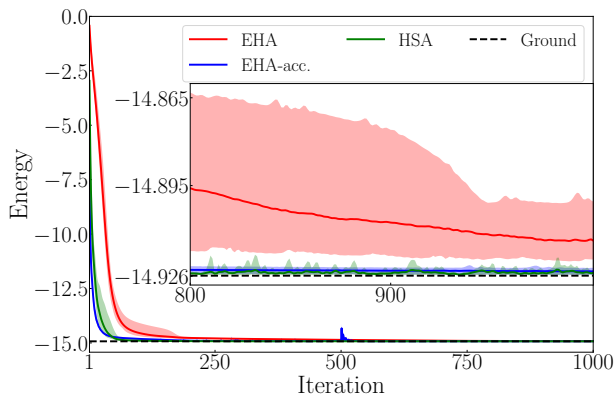


FIG. 7. Comparison between our EHA and HSA for TFIM in Eq. (10). Although HSA outperforms EHA, the performance of EHA with acceleration is similar to that of HSA.

2. Quantum chemistry problems

Now we compare our EHA with chemically inspired ansatzes UCCSD and GRSD by focusing on the HF molecule and H_3^+ cation. The quantum circuits for UCCSD and GRSD are much more complicated than our EHA. To be specific, from Fig. 2 and Fig. 3, the entangling gates in our EHA are all local CX gates that are applied to nearest-neighbor qubits. However, when realizing UCCSD, it has some non-local CX gates, while for GRSD, in addition to non-local CX gates, it has some T gates. We list the number of all CX gates, non-local CX gates and T gates of UCCSD and GRSD for the HF molecule and H_3^+ cation in Table IV (Appendix C). Since most current hardware platforms only allow nearest-neighbor connections [73, 74], and the use of T gates causes a very high cost [75], our EHA is much easier to be realized with current NISQ devices compared to UCCSD and GRSD. Thus, in the following we only focus on the performance of EHA, UCCSD and GRSD without assuming that they have roughly the same number of CX gates.

Recall that we adopt PennyLane to simulate UCCSD and GRSD (referred to as ALLSD in PennyLane). For both of them, we start with the Hartree-Fock state [28]. For our EHA, we project the final output states to the feasible state space, which is spanned by the states considering all single and double excitations above the Hartree-Fock state. We show that our EHA is superior to both of them in robustly obtaining a lower energy.

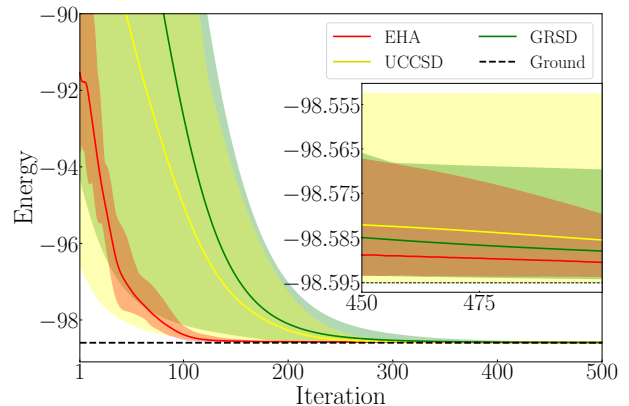


FIG. 8. Comparison of our EHA with UCCSD and GRSD for HF. The black dashed line denotes the ground energy of the HF Hamiltonian obtained by second quantization. Our EHA can robustly achieve a lower average energy as compared to UCCSD and GRSD.

As for the HF molecule, its bond length is set to be 1.1. Our EHA consists of 12 qubits and has 18 blocks. We demonstrate the experimental results in Fig. 8. Here, the black dashed baseline denotes the ground energy of the HF Hamiltonian obtained by second quantization. We find that our EHA can achieve a lower energy on average and its performance is more robust with respect

to different realizations compared to UCCSD and GRSD. While for the best performance among 10 realizations, UCCSD and GRSD are slightly superior to our EHA.

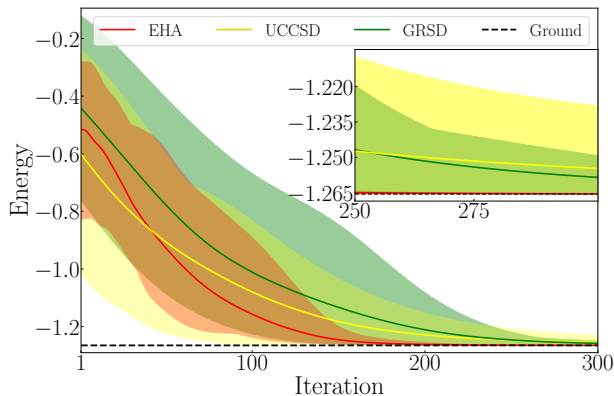


FIG. 9. Comparison of our EHA with UCCSD and GRSD for H_3^+ . The black dashed line denotes the ground energy of the second quantization Hamiltonian of H_3^+ . Our EHA can always achieve the ground energy.

As for the H_3^+ cation, we need to modify the cost function Eq. (3) by adding a penalty term for our EHA. The reason is as follows. On the one hand the second quantization Hamiltonian of H_3^+ depends only on the spin-orbital basis, and is independent of the number of electrons [65]. On the other hand, in contrast to UCCSD and GRSD, our EHA does not preserve particle numbers. Therefore, if there is no constraint, under EHA the trial states will converge to the ground state of H_3 having 3 electrons, while H_3^+ has only 2 electrons. To address this issue, we can simply add a constraint on the number of electrons by means of penalty function. Specifically, we consider the cost function as

$$C(\theta) = \langle \psi(\theta) | H | \psi(\theta) \rangle + \beta [\langle \psi(\theta) | N | \psi(\theta) \rangle - 2]^2. \quad (11)$$

Here, H is the Hamiltonian of H_3^+ , β is the penalty hyperparameter, and $N = \sum_{\alpha} \hat{c}_{\alpha}^{\dagger} \hat{c}_{\alpha}$ denotes the number operator with $\hat{c}_{\alpha}^{\dagger}$ and \hat{c}_{α} being the particle creation and annihilation operators, respectively, and the index α running over the basis of single-particle. Here, for H_3^+ , the bond length is set to be 1.1. Our EHA consists of 6 qubits and has 9 blocks, and the hyperparameter $\beta = 10$. The experimental results are shown in Fig. 9. We find that our EHA is much better than UCCSD and GRSD, as EHA can always achieve the ground energy for different realizations.

C. Ability to quickly adjust entanglement

Recall that to solve the ground state problem, it is imperative to generate a quantum state with the matched entanglement. In this subsection, we demonstrate that because of the variational entangler design in our EHA,

it can rapidly adjust the entanglement to the required amount during the training process.

For an N -qubit system state ρ , denote by ρ_i the state of the i -th qubit by taking partial trace over all the other qubits, namely, $\rho_i = \text{Tr}_{\bar{i}}[\rho]$, where \bar{i} denotes the subsystem excluding the i -th qubit. Here, we adopt the average von Neumann entropy

$$S \triangleq -\frac{1}{N} \sum_{i=1}^N \text{Tr}[\rho_i \log(\rho_i)]$$

to be the figure of merit for evaluating the entanglement of quantum state ρ .

For models already investigated in Subsection III B, we now investigate their entanglement transitions of the generated trial states under different ansatzes during the optimization. In the following figures of this subsection, the black dashed line denotes the entanglement of the ground state, and the other lines denote the respective average value of the entanglement over 10 realizations under different ansatzes.

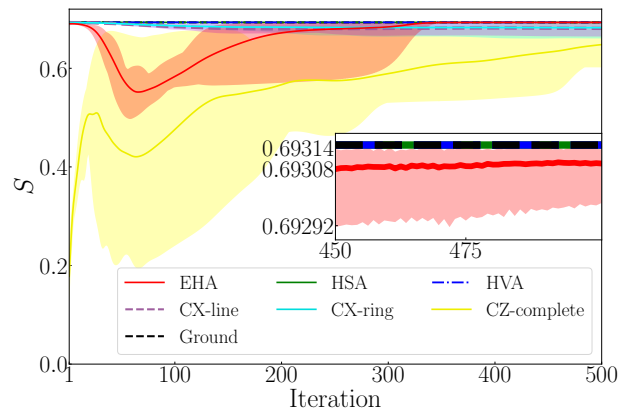


FIG. 10. Entanglement transitions under different ansatzes for HM in Eq. (8). Our EHA can quickly adjust the entanglement to the desired amount.

For the 12-qubit HM in Eq. (8), we illustrate the entanglement transitions (corresponding to Fig. 4) in Fig. 10. We find that the ground state has a large amount of entanglement. Under HVA and HSA, the entanglement of the generated quantum states stays at the same value as the desired amount during the optimization. This validates that for the problem-specific HVA and HSA, they only explore specific spaces of the unitaries during training. This is the main reason that HVA and HSA usually outperform problem-agnostic HEAs. However, as we mentioned, the performance of HSA and HVA depends heavily on the initial reference states (see Appendix D), which are often hard to determine. For problem-agnostic HEAs, it is clear that our EHA can rapidly adjust the entanglement to the desired level, while the other HEAs cannot. This is owing to the variational entangler design in our EHA.

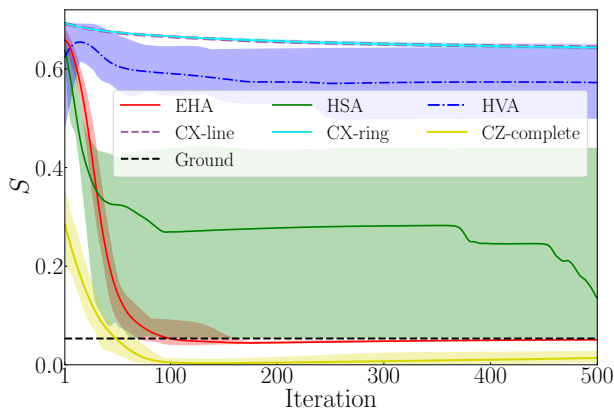


FIG. 11. Entanglement transitions under different ansatzes for TFIM in Eq. (9). Our EHA is much better than other ansatzes in adjusting the entanglement to the required amount.

For the 12-qubit TFIM in Eq. (9), we illustrate the entanglement transitions (corresponding to Fig. 5) in Fig. 11. We find that in this case the entanglement of the ground state is low. Under our EHA, the excess entanglement can be quickly removed and adjusted to the desired amount, which is hard to do with other ansatzes. The robustness of the entanglement transitions under different realizations is particularly poor for HSA.

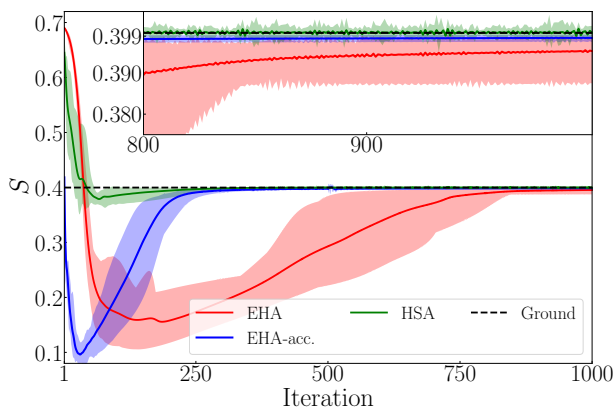


FIG. 12. Entanglement transitions under HSA, EHA and EHA-acc. for TFIM in Eq. (10).

As for the TFIM in Eq. (10), we demonstrate the entanglement transitions under EHA and HSA in Fig. 12. From Fig. 7 and Fig. 12, we find that in this case HSA is superior to our EHA, as it can adjust the entanglement to the required level in a much quicker way. However, we note that the accelerated version of EHA can also tune the entanglement to the required level quickly.

For the H_3^+ cation, the entanglement transitions under EHA, UCCSD and GRSD (corresponding to Fig. 9) are shown in Fig. 13. Here, we only depict the average value of the entanglement over 10 realizations. We find that as compared with UCCSD and GRSD, EHA can quickly

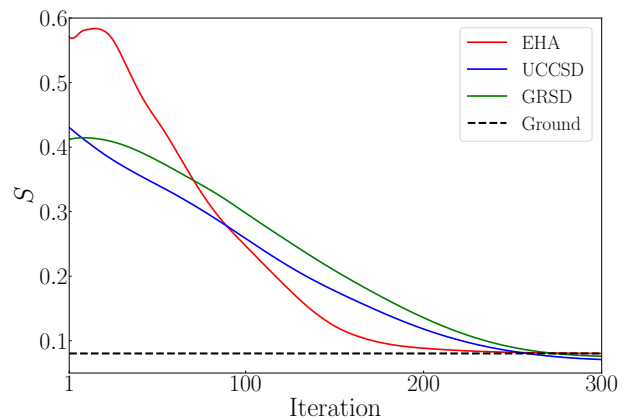


FIG. 13. Entanglement transitions under EHA, UCCSD and GRSD for H_3^+ .

adjust the entanglement to the desired level.

D. The impact of initial reference states

In this subsection, we consider the impact of initial reference states on our EHA. Since the reference state in quantum chemistry problems is typically chosen as Hartree-Fock state, we only concern quantum many-body systems. Moreover, for problem-specific ansatzes like HSA and HVA, the selection of initial reference states has strict requirements. Taking the HSA as an example, starting from an initial state that violates the symmetry of the Hamiltonian will automatically create a bias against HSA resulting in poor performance. This has been illustrated in Fig. 23 (Appendix D). Therefore, we analyze the impact of different initial reference states on ansatzes only by comparing the performance of EHA and HEA. Note that in the above experiments, among the three considered HEAs, the CZ-complete performs best. We now compare EHA with CZ-complete under different initial reference states.

We consider three typical initial reference states: $\otimes^{12}|0\rangle$, $\otimes^{12}|+\rangle$ and $\otimes^6|\Psi^-\rangle$. The experimental results for HM in Eq. (8) and TFIM in Eq. (9) are demonstrated in Fig. 14 and Fig. 15, respectively. We find that for both HM and TFIM, our EHA is superior to CZ-complete, and the performance of EHA is more robust under different initial reference states. The phenomenon can be explained by checking the corresponding entanglement transitions. As an illustration, we demonstrate the entanglement transitions of HM (corresponding to Fig. 14) in Fig. 16. It is clear that compared to CZ-complete, our EHA can robustly and quickly adjust the entanglement to the desired level under different initial states. This is due to the variational design in EHA, which also makes EHA a strong candidate for quantum computing.

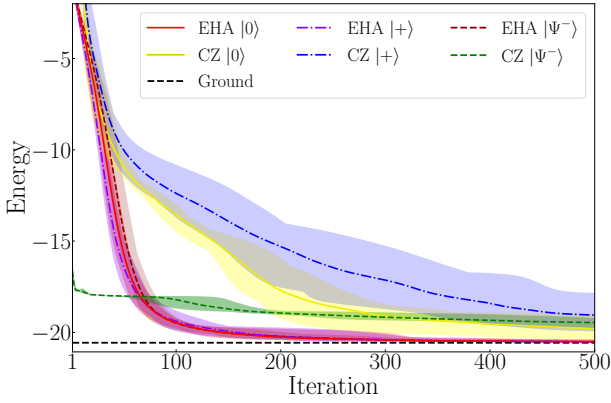


FIG. 14. Comparison between our EHA and CZ-complete under different initial reference states for HM in Eq. (8). The performance of our EHA is more robust than CZ-complete.

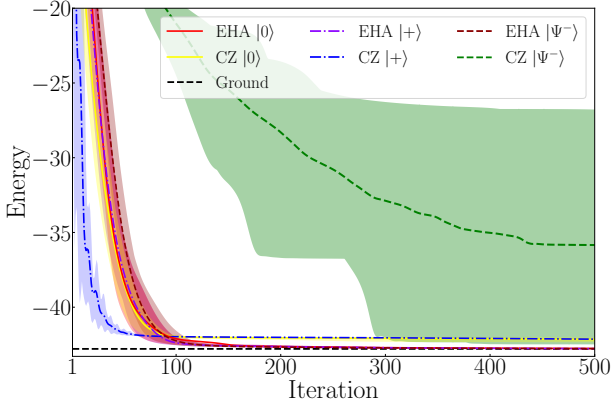


FIG. 15. Comparison between our EHA and CZ-complete under different initial reference states for TFIM in Eq. (9). The performance of our EHA is more robust than CZ-complete.

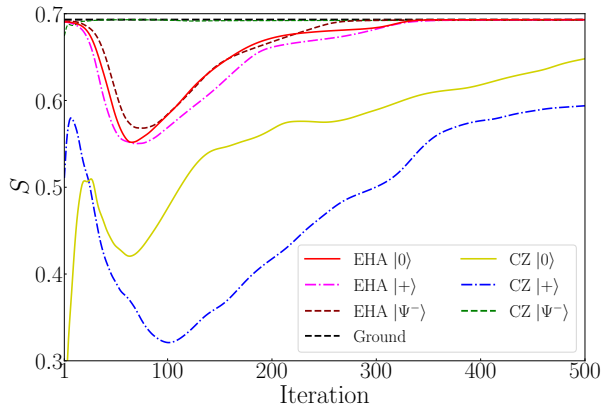


FIG. 16. Entanglement transitions of EHA and CZ-complete under different initial reference states for HM in Eq. (8). The black dashed line denotes the entanglement of the ground state. Other lines denote the respective average value of the entanglement over 10 realizations. The entanglement transitions of our EHA are more robust than CZ-complete under different initial states.

E. Avoiding BP with reduced-domain initialization

In this subsection, we consider how to train our EHA with relatively large blocks.

As illustrated in Fig. 2 and Fig. 3, our EHA utilizes a total number of $6(N-1)$ CX gates per block. This makes the expressibility of EHA grow quickly as the number of blocks L increases. However, it is well known that too expressive ansatz will result in the phenomenon of BP, making the training extremely difficult. Therefore, our EHA may suffer from BP when L is large.

There have been many ways to mitigate the impact of BP [30, 31, 76–79]. Here, we adopt the reduced-domain method introduced in [30]. It was stated that to balance the conflict between trainability and expressibility of PQCs, the domain of each variational parameter should be reduced in proportion to $\frac{1}{\sqrt{L}}$, where L denotes the depth of PQC [30]. We demonstrate that the reduced-domain initialization [30] can help train our EHA with relatively large blocks.

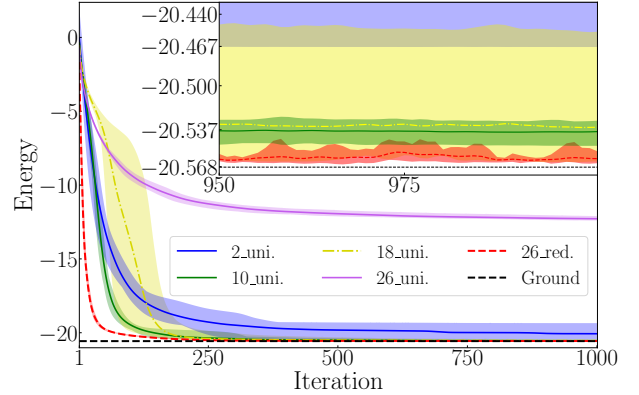


FIG. 17. Performance of EHA under different numbers of blocks and initializations for HM in Eq. (8). With the reduced-domain initialization, the 26-block circuit can generate quantum states closer to the ground state in a faster way compared to other schemes.

We focus on the 12-qubit HM in Eq. (8), and consider four different numbers of blocks, namely, $L = 2, 10, 18$ and 26. The experimental settings are the same as those in Subsection III B, except for the initialization.

We first draw the variational parameters according to the uniform distribution $\mathcal{U}[-\pi, \pi]$ as we have done in Subsection III B. The numerical results are illustrated in Fig 17. We find that the 10-block EHA has the best performance among the four considered cases, as it robustly converges to a lower energy. As compared with the 10-block EHA, the 2-block EHA is less expressible and cannot obtain better performance, while the 18-block EHA is more expressible but difficult to be trained [46], which is indicated by the slower convergence rate and larger sample variance. The 26-block EHA is too expressive to be trained. To address the training issue for large blocks of EHA, we leverage the reduced-domain

initialization method [30]. Specifically, each variational parameter is drawn according to a reduced uniform distribution $\mathcal{U}[\frac{\pi}{2} - \frac{1}{\sqrt{L}}, \frac{\pi}{2} + \frac{1}{\sqrt{L}}]$. The performance of the 26-block reduced version of EHA is plotted in Fig. 17. We find that with the reduced uniform initialization, the 26-block EHA has a much faster convergence rate, higher level of accuracy and robustness with respect to different realizations, as compared with other cases.

F. Performance Testing

In this subsection, we focus on the performance of our EHA on additional quantum chemistry and quantum many-body models.

We first compare our EHA with an ansatz termed adaptive derivative-assembled pseudo-Trotter ansatz variational quantum eigensolver (ADAPT-VQE), which was proposed in [22] for molecular simulations. The key idea of ADAPT-VQE is to systematically grow the ansatz by adding fermionic operators one at a time to maximally recover the correlation energy at each step. The initial reference state of ADAPT-VQE is also the Hartree-Fock state, and the operator pool includes all single and double excitation operators acting on the reference state without flipping the spin of the excited particles. We list the number of all CX gates, non-local CX gates and T gates of ADAPT-VQE for different molecules in Table IV (Appendix C). It has been shown that ADAPT-VQE outperforms UCC in terms of both circuit depth and chemical accuracy [22].

For all molecules, the ADAPT-VQE results in this paper are obtained by PennyLane, with the termination condition being gradient less than 10^{-3} . While for our EHA, we find that for all experiments, the gradient is never below 10^{-3} before the end of training. This implies that the gradient of EHA is larger than ADAPT-VQE before the end of the optimization. Moreover, for all molecules, we have checked that the spin and particle number of the solutions obtained by both ADAPT-VQE and EHA are the same as the actual states.

We first consider solving the ground state of H_5 at different bond lengths. Here, we consider the target ground state with $s_z = \frac{1}{2}$. Our EHA consists of 10 qubits, $L = 38$ blocks, and the initial parameters are drawn from a reduced uniform distribution $\mathcal{U}[\frac{\pi}{2} - \frac{1}{\sqrt{L}}, \frac{\pi}{2} + \frac{1}{\sqrt{L}}]$. To guarantee the obtained state having $s_z = \frac{1}{2}$, similar to what we have done in dealing with H_3^+ , we add an S_z penalty term (with the hyperparameter being 100) in the cost function in our EHA. We perform 2000 iterations, with the step size being 0.1 for the first 500 iterations, and 0.001 for the last 1500 iterations. We take the minimum energy during the training process as the approximate solution of the ground energy. We illustrate the ground energy error in Fig. 18. We find that when the bond length is larger than 1.1, the ground energy error obtained by ADAPT-VQE exceeds the chemical accuracy

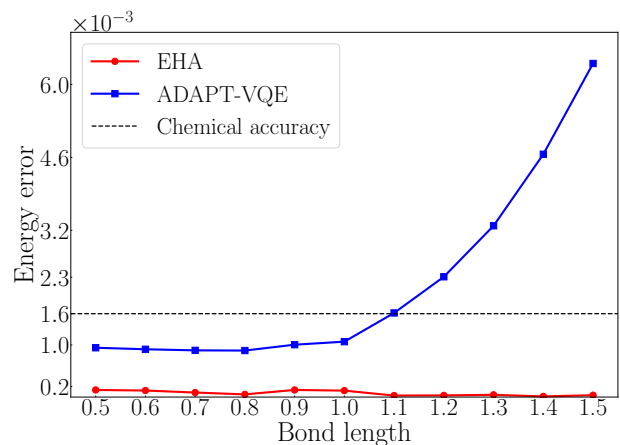


FIG. 18. Ground energy error of EHA and ADAPT-VQE for H_5 . The energy error obtained by ADAPT-VQE exceeds the chemical accuracy and grows quickly when the bond length is larger than 1.1. While for our EHA, the energy error stays nearly at the same value as the bond length increases, and is about 1/8 of the chemical accuracy.

(1.6×10^{-3}) [80] and grows quickly as the bond length increases. While for our EHA, the energy error remains nearly constant as the bond length increases, and is lower than ADAPT-VQE. Specifically, the ground energy error can maintain about 1/8 of the chemical accuracy for bond length ranging from 0.5 to 1.5.

We now apply our EHA and ADAPT-VQE to other molecules. For our EHA we perform at most 3000 iterations, and for different molecules the step size schedules are illustrated in Table V (Appendix E). The results are demonstrated in Table II. The first column lists the molecules with the bond length in parentheses, the second column shows the number of qubits needed after second quantization of the molecules, and the third column lists the blocks of our EHA. We also list the best value, mean value and the standard deviation (STD) of the energy obtained by our EHA in Table II. It is clear that our EHA outperforms ADAPT-VQE and has less than 5×10^{-5} standard deviation.

We further apply our EHA on other quantum many-body systems, where their corresponding step size schedules are illustrated in Table V (Appendix E). We demonstrate the results in Table III. The first column lists the models with the number of qubits in parentheses, where the HM, TFIM1 and TFIM2 are described by Eq. (8), Eq. (9) and Eq. (10) respectively. Here, the BHM denotes the Bose-Hubbard model (BHM) [81] in a chain lattice, whose Hamiltonian reads

$$H = - \left(\sum_{i=1}^{N-1} \hat{b}_i^\dagger \hat{b}_{i+1} + \text{h.c.} \right) + 7 \sum_{i=1}^N \hat{n}_i (\hat{n}_i - 1), \quad (12)$$

where \hat{b}_i^\dagger and \hat{b}_i denote the Bosonic creation and annihilation operators on site i , respectively, and $\hat{n}_i = \hat{b}_i^\dagger \hat{b}_i$ denotes the number operator of site i . For BHM, we can

Model	Qubits	Blocks	Ground energy	ADAPT-VQE energy	EHA-best	EHA-mean	EHA-STD
BeH ₂ (1.1)	14	32	-15.5496	-15.5490	-15.5490	-15.5490	0.0000
LiH(1.11)	12	16	-7.8288	-7.8282	-7.8286	-7.8286	0.0000
HF(1.1)	12	18	-98.5951	-98.5942	-98.5948	-98.5947	0.0000

TABLE II. Performance of EHA and ADAPT-VQE for different molecules.

Model	Blocks	Ground energy	Energy-best	Energy-mean	Energy-STD	Fidelity-best	Fidelity-mean	Fidelity-STD
HM(8)	14	-13.4997	-13.4994	-13.4993	0.0001	1.0000	1.0000	0.0000
HM(12)	28	-20.5684	-20.5679	-20.5675	0.0002	1.0000	0.9999	0.0000
HM(16)	42	-27.6469	-27.6461	-27.6459	0.0002	0.9999	0.9999	0.0000
TFIM1(8)	6	-20.5018	-20.5018	-20.5015	0.0004	1.0000	1.0000	0.0000
TFIM1(12)	6	-42.7890	-42.7889	-42.7880	0.0010	1.0000	1.0000	0.0000
TFIM1(16)	8	-57.0763	-57.0760	-57.0759	0.0002	1.0000	1.0000	0.0000
TFIM2(8)	8	-9.8380	-9.8378	-9.8376	0.0002	1.0000	0.9999	0.0000
TFIM2(12)	12	-14.9260	-14.9257	-14.9255	0.0002	1.0000	0.9999	0.0000
TFIM2(16)	20	-20.0164	-20.0160	-20.0156	0.0003	0.9999	0.9999	0.0000
BHM(8)	12	0.0000	0.0001	0.0002	0.0001	1.0000	1.0000	0.0000
BHM(16)	20	0.0000	0.0001	0.0002	0.0001	1.0000	1.0000	0.0000

TABLE III. Performance of EHA for different quantum many-body systems.

use binary Bosonic mapping [82] to transform the Hamiltonian in Eq. (12) into the form of a linear combination of Pauli strings, which is done by utilizing PennyLane in this paper. The number of blocks in our EHA is listed in the second column. In Table III, we list the best value, mean value and the standard deviation of the energy and fidelity obtained by our EHA. We find that for all cases, our EHA can attain the ground energy with a very high level of accuracy. In the best case, the ground energy error is less than 1×10^{-3} , and on average the ground energy error is less than the chemical accuracy of 1.6×10^{-3} . Moreover, the standard deviation is very small, which is at most 1×10^{-3} . The fidelity with the ground state is no smaller than 99.99% on average, and the standard deviation is lower than 5×10^{-5} .

IV. Conclusion

In this paper, we propose an efficient hardware-efficient ansatz, EHA, for eigensolvers, in which the entanglers

are designed to be variational rather than fixed. This entanglement-variational design allows the circuit to rapidly adjust the entanglement of the generated trial states to the required amount, and in turn greatly enhance the performance. We have demonstrated that our EHA can find approximate solutions for eigensolvers with a very high level of accuracy, and its performance is robust to choices of initial reference states and different realizations. We believe that our EHA is particularly suitable for NISQ era and will generate wide impact on developing algorithms with potential quantum advantages for various practical applications.

-
- [1] Hsin-Yuan Huang, Richard Kueng, Giacomo Torlai, Victor V. Albert, and John Preskill, “Provably efficient machine learning for quantum many-body problems,” *Science* **377**, eabk3333 (2022).
- [2] I. Stetcu, A. Baroni, and J. Carlson, “Variational approaches to constructing the many-body nuclear ground state for quantum computing,” *Phys. Rev. C* **105**, 064308 (2022).
- [3] Alan Morningstar, Markus Hauru, Jackson Beall, Martin Ganahl, Adam G.M. Lewis, Vedika Khemani, and Guifre Vidal, “Simulation of quantum many-body dynamics with Tensor Processing Units: Floquet prethermalization,” *PRX Quantum* **3**, 020331 (2022).
- [4] Sam McArdle, Suguru Endo, Alán Aspuru-Guzik, Simon C. Benjamin, and Xiao Yuan, “Quantum computational chemistry,” *Rev. Mod. Phys.* **92**, 015003 (2020).
- [5] Vincent E. Elfving, Marta Millaruelo, José A. Gámez, and Christian Gogolin, “Simulating quantum chemistry in the seniority-zero space on qubit-based quantum computers,” *Phys. Rev. A* **103**, 032605 (2021).
- [6] Changsu Cao, Jiaqi Hu, Wengang Zhang, Xusheng Xu, Dechin Chen, Fan Yu, Jun Li, Han-Shi Hu, Dingshun Lv,

- and Man-Hong Yung, “Progress toward larger molecular simulation on a quantum computer: Simulating a system with up to 28 qubits accelerated by point-group symmetry,” *Phys. Rev. A* **105**, 062452 (2022).
- [7] Bela Bauer, Sergey Bravyi, Mario Motta, and Garnet Kin-Lic Chan, “Quantum algorithms for quantum chemistry and quantum materials science,” *Chem. Rev.* **120**, 12685–12717 (2020).
- [8] He Ma, Marco Govoni, and Giulia Galli, “Quantum simulations of materials on near-term quantum computers,” *npj Comput. Mater.* **6**, 85 (2020).
- [9] Lindsay Bassman, Miroslav Urbanek, Mekena Metcalf, Jonathan Carter, Alexander F. Kemper, and Wibe A. de Jong, “Simulating quantum materials with digital quantum computers,” *Quantum Sci. Technol.* **6**, 043002 (2021).
- [10] Daniel J. Egger, Claudio Gambella, Jakub Marecek, Scott McFaddin, Martin Mevissen, Rudy Raymond, Andrea Simonetto, Stefan Woerner, and Elena Yndurain, “Quantum computing for finance: State-of-the-art and future prospects,” *IEEE Trans. Quantum Eng.* **1**, 3101724 (2020).
- [11] M. Cerezo, Guillaume Verdon, Hsin-Yuan Huang, Lukasz Cincio, and Patrick J. Coles, “Challenges and opportunities in quantum machine learning,” *Nat. Comput. Sci.* **2**, 567–576 (2022).
- [12] John Preskill, “Quantum Computing in the NISQ era and beyond,” *Quantum* **2**, 79 (2018).
- [13] Kishor Bharti *et al.*, “Noisy intermediate-scale quantum algorithms,” *Rev. Mod. Phys.* **94**, 015004 (2022).
- [14] Kishor Bharti, Tobias Haug, Vlatko Vedral, and Leong-Chuan Kwek, “Noisy intermediate-scale quantum algorithm for semidefinite programming,” *Phys. Rev. A* **105**, 052445 (2022).
- [15] Alberto Peruzzo, Jarrod McClean, Peter Shadbolt, Man-Hong Yung, Xiao-Qi Zhou, Peter J. Love, Alán Aspuru-Guzik, and Jeremy L. O’Brien, “A variational eigenvalue solver on a photonic quantum processor,” *Nat. Commun.* **5**, 4213 (2014).
- [16] M. Cerezo *et al.*, “Variational quantum algorithms,” *Nat. Rev. Phys.* **3**, 625–644 (2021).
- [17] Jules Tilly *et al.*, “The variational quantum eigensolver: a review of methods and best practices,” *Phys. Rep.* **986**, 1–128 (2022).
- [18] Joris Kattemölle and Jasper van Wezel, “Variational quantum eigensolver for the Heisenberg antiferromagnet on the kagome lattice,” *Phys. Rev. B* **106**, 214429 (2022).
- [19] Andy C. Y. Li *et al.*, “Benchmarking variational quantum eigensolvers for the square-octagon-lattice Kitaev model,” *Phys. Rev. Res.* **5**, 033071 (2023).
- [20] Adam Callison and Nicholas Chancellor, “Hybrid quantum-classical algorithms in the noisy intermediate-scale quantum era and beyond,” *Phys. Rev. A* **106**, 010101 (2022).
- [21] Mateusz Ostaszewski, Edward Grant, and Marcello Benedetti, “Structure optimization for parameterized quantum circuits,” *Quantum* **5**, 391 (2021).
- [22] Harper R. Grimsley, Sophia E. Economou, Edwin Barnes, and Nicholas J. Mayhall, “An adaptive variational algorithm for exact molecular simulations on a quantum computer,” *Nat. Commun.* **10**, 3007 (2019).
- [23] Ho Lun Tang, V.O. Shkolnikov, George S. Barron, Harper R. Grimsley, Nicholas J. Mayhall, Edwin Barnes, and Sophia E. Economou, “qubit-ADAPT-VQE: An adaptive algorithm for constructing hardware-efficient ansätze on a quantum processor,” *PRX Quantum* **2**, 020310 (2021).
- [24] Mateusz Ostaszewski, Lea M. Trenkwalder, Wojciech Masarczyk, Eleanor Scerri, and Vedran Dunjko, “Reinforcement learning for optimization of variational quantum circuit architectures,” *Advances in Neural Information Processing Systems* **34**, 18182–18194 (2021).
- [25] Yuxuan Du, Tao Huang, Shan You, Min-Hsiu Hsieh, and Dacheng Tao, “Quantum circuit architecture search for variational quantum algorithms,” *npj Quantum Inf.* **8**, 62 (2022).
- [26] Li Ding and Lee Spector, “Evolutionary quantum architecture search for parametrized quantum circuits,” in *Proceedings of the Genetic and Evolutionary Computation Conference Companion* (2022) pp. 2190–2195.
- [27] Harper R. Grimsley, George S. Barron, Edwin Barnes, Sophia E. Economou, and Nicholas J. Mayhall, “Adaptive, problem-tailored variational quantum eigensolver mitigates rough parameter landscapes and barren plateaus,” *npj Quantum Inf.* **9**, 19 (2023).
- [28] Google AI Quantum, Collaborators*†, *et al.*, “Hartree-Fock on a superconducting qubit quantum computer,” *Science* **369**, 1084–1089 (2020).
- [29] Chris Cade, Lana Mineh, Ashley Montanaro, and Stasja Stanisic, “Strategies for solving the Fermi-Hubbard model on near-term quantum computers,” *Phys. Rev. B* **102**, 235122 (2020).
- [30] Yabo Wang, Bo Qi, Chris Ferrie, and Daoyi Dong, “Trainability enhancement of parameterized quantum circuits via reduced-domain parameter initialization,” *arXiv preprint arXiv:2302.06858* (2023).
- [31] Kaining Zhang, Liu Liu, Min-Hsiu Hsieh, and Dacheng Tao, “Escaping from the barren plateau via gaussian initializations in deep variational quantum circuits,” *Advances in Neural Information Processing Systems* **35**, 18612–18627 (2022).
- [32] James Stokes, Josh Izaac, Nathan Killoran, and Giuseppe Carleo, “Quantum Natural Gradient,” *Quantum* **4**, 269 (2020).
- [33] Alicia B. Magann, Kenneth M. Rudinger, Matthew D. Grace, and Mohan Sarovar, “Feedback-based quantum optimization,” *Phys. Rev. Lett.* **129**, 250502 (2022).
- [34] Shi-Xin Zhang, Zhou-Quan Wan, Chee-Kong Lee, Chang-Yu Hsieh, Shengyu Zhang, and Hong Yao, “Variational quantum-neural hybrid eigensolver,” *Phys. Rev. Lett.* **128**, 120502 (2022).
- [35] Nicholas H. Stair and Francesco A. Evangelista, “Simulating many-body systems with a projective quantum eigensolver,” *PRX Quantum* **2**, 030301 (2021).
- [36] Alba Cervera-Lierta, Jakob S. Kottmann, and Alán Aspuru-Guzik, “Meta-variational quantum eigensolver: Learning energy profiles of parameterized Hamiltonians for quantum simulation,” *PRX Quantum* **2**, 020329 (2021).
- [37] Keisuke Fujii, Kaoru Mizuta, Hiroshi Ueda, Kosuke Mitarai, Wataru Mizukami, and Yuya O. Nakagawa, “Deep variational quantum eigensolver: a divide-and-conquer method for solving a larger problem with smaller size quantum computers,” *PRX Quantum* **3**, 010346 (2022).
- [38] Tobias Haug, Kishor Bharti, and M. S. Kim, “Capacity and quantum geometry of parametrized quantum circuits,” *PRX Quantum* **2**, 040309 (2021).

- [39] Sukin Sim, Peter D. Johnson, and Alán Aspuru-Guzik, “Expressibility and entangling capability of parameterized quantum circuits for hybrid quantum-classical algorithms,” *Adv. Quantum Technol.* **2**, 1900070 (2019).
- [40] Abhinav Kandala, Antonio Mezzacapo, Kristan Temme, Maika Takita, Markus Brink, Jerry M. Chow, and Jay M. Gambetta, “Hardware-efficient variational quantum eigensolver for small molecules and quantum magnets,” *Nature* **549**, 242–246 (2017).
- [41] Maria Schuld, Alex Bocharov, Krysta M. Svore, and Nathan Wiebe, “Circuit-centric quantum classifiers,” *Phys. Rev. A* **101**, 032308 (2020).
- [42] Boy Choy and David J. Wales, “Molecular energy landscapes of hardware-efficient ansatzes in quantum computing,” *J. Chem. Theory Comput.* **19**, 1197–1206 (2023).
- [43] Lennart Bittel and Martin Kliesch, “Training variational quantum algorithms is NP-hard,” *Phys. Rev. Lett.* **127**, 120502 (2021).
- [44] Eric R. Anschuetz and Bobak T. Kiani, “Quantum variational algorithms are swamped with traps,” *Nat. Commun.* **13**, 7760 (2022).
- [45] Jarrod R. McClean, Sergio Boixo, Vadim N. Smelyanskiy, Ryan Babbush, and Hartmut Neven, “Barren plateaus in quantum neural network training landscapes,” *Nat. Commun.* **9**, 4812 (2018).
- [46] Zoë Holmes, Kunal Sharma, M. Cerezo, and Patrick J. Coles, “Connecting ansatz expressibility to gradient magnitudes and barren plateaus,” *PRX Quantum* **3**, 010313 (2022).
- [47] Yanzhu Chen, Linghua Zhu, Nicholas J. Mayhall, Edwin Barnes, and Sophia E. Economou, “How much entanglement do quantum optimization algorithms require?” in *Quantum 2.0* (Optica Publishing Group, 2022) pp. QM4A–2.
- [48] Andreas J. C. Woitzik, Panagiotis Kl. Barkoutsos, Filip Wudarski, Andreas Buchleitner, and Ivano Tavernelli, “Entanglement production and convergence properties of the variational quantum eigensolver,” *Phys. Rev. A* **102**, 042402 (2020).
- [49] Carlos Ortiz Marrero, Mária Kieferová, and Nathan Wiebe, “Entanglement-induced barren plateaus,” *PRX Quantum* **2**, 040316 (2021).
- [50] Lorenzo Leone, Salvatore F. E. Oliviero, Lukasz Cincio, and M. Cerezo, “On the practical usefulness of the Hardware Efficient Ansatz,” *arXiv preprint arXiv:2211.01477* (2022).
- [51] Roeland Wiersema, Cunlu Zhou, Yvette de Sereville, Juan Felipe Carrasquilla, Yong Baek Kim, and Henry Yuen, “Exploring entanglement and optimization within the Hamiltonian Variational Ansatz,” *PRX Quantum* **1**, 020319 (2020).
- [52] Chufan Lyu, Xusheng Xu, Man-Hong Yung, and Abolfazl Bayat, “Symmetry enhanced variational quantum spin eigensolver,” *Quantum* **7**, 899 (2023).
- [53] Jonathan Romero, Ryan Babbush, Jarrod R. McClean, Cornelius Hempel, Peter J. Love, and Alán Aspuru-Guzik, “Strategies for quantum computing molecular energies using the unitary coupled cluster ansatz,” *Quantum Sci. Technol.* **4**, 014008 (2018).
- [54] Rodney J. Bartlett and Monika Musiał, “Coupled-cluster theory in quantum chemistry,” *Rev. Mod. Phys.* **79**, 291 (2007).
- [55] Juan Miguel Arrazola, Olivia Di Matteo, Nicolás Quesada, Soran Jahangiri, Alain Delgado, and Nathan Killo-
ran, “Universal quantum circuits for quantum chemistry,” *Quantum* **6**, 742 (2022).
- [56] Roland C. Farrell, Marc Illa, Anthony N. Ciavarella, and Martin J. Savage, “Scalable circuits for preparing ground states on digital quantum computers: The schwinger model vacuum on 100 qubits,” *arXiv preprint arXiv:2308.04481* (2023).
- [57] Zhenyu Cai, “Resource estimation for quantum variational simulations of the Hubbard model,” *Phys. Rev. Appl.* **14**, 014059 (2020).
- [58] Mårten Skogh, Oskar Leinonen, Phalgun Lolur, and Martin Rahm, “Accelerating variational quantum eigensolver convergence using parameter transfer,” *Electronic Structure* **5**, 035002 (2023).
- [59] Manpreet Singh Jattana, Fengping Jin, Hans De Raedt, and Kristel Michiels, “Improved variational quantum eigensolver via quasidynamical evolution,” *Phys. Rev. Appl.* **19**, 024047 (2023).
- [60] Joonho Kim, Jaedeok Kim, and Dario Rosa, “Universal effectiveness of high-depth circuits in variational eigenproblems,” *Phys. Rev. Res.* **3**, 023203 (2021).
- [61] Farrokh Vatan and Colin Williams, “Optimal quantum circuits for general two-qubit gates,” *Phys. Rev. A* **69**, 032315 (2004).
- [62] Alán Aspuru-Guzik, Anthony D. Dutoi, Peter J. Love, and Martin Head-Gordon, “Simulated quantum computation of molecular energies,” *Science* **309**, 1704–1707 (2005).
- [63] Trygve Helgaker, Sonia Coriani, Poul Jørgensen, Kasper Kristensen, Jeppe Olsen, and Kenneth Ruud, “Recent advances in wave function-based methods of molecular-property calculations,” *Chem. Rev.* **112**, 543–631 (2012).
- [64] Ryan Babbush, Dominic W. Berry, Ian D. Kivlichan, Annie Y. Wei, Peter J. Love, and Alán Aspuru-Guzik, “Exponentially more precise quantum simulation of fermions in second quantization,” *New J. Phys.* **18**, 033032 (2016).
- [65] Trygve Helgaker, Poul Jørgensen, and Jeppe Olsen, *Molecular electronic-structure theory* (John Wiley and Sons, 2013).
- [66] Michael A. Nielsen, “The fermionic canonical commutation relations and the Jordan-Wigner transform,” *School of Physical Sciences The University of Queensland* **59** (2005).
- [67] Jarrod R. McClean *et al.*, “OpenFermion: the electronic structure package for quantum computers,” *Quantum Sci. Technol.* **5**, 034014 (2020).
- [68] Ville Bergholm *et al.*, “PennyLane: Automatic differentiation of hybrid quantum-classical computations,” *arXiv preprint arXiv:1811.04968* (2018).
- [69] S. Debnath, N. M. Linke, C. Figgatt, K. A. Landsman, K. Wright, and C. Monroe, “Demonstration of a small programmable quantum computer with atomic qubits,” *Nature* **536**, 63–66 (2016).
- [70] Martin Larocca, Nathan Ju, Diego García-Martín, Patrick J. Coles, and Marco Cerezo, “Theory of overparametrization in quantum neural networks,” *Nat. Comput. Sci.* **3**, 542–551 (2023).
- [71] Jason D. Lee, Max Simchowitz, Michael I. Jordan, and Benjamin Recht, “Gradient descent only converges to minimizers,” in *Conference on learning theory* (PMLR, 2016) pp. 1246–1257.
- [72] Charles R. Harris *et al.*, “Array programming with NumPy,” *Nature* **585**, 357–362 (2020).

- [73] Norbert M. Linke, Dmitri Maslov, Martin Roetteler, Shantanu Debnath, Caroline Figgatt, Kevin A. Landsman, Kenneth Wright, and Christopher Monroe, “Experimental comparison of two quantum computing architectures,” *Proc. Natl. Acad. Sci. U.S.A* **114**, 3305–3310 (2017).
- [74] Sajjad Sanaei and Naser Mohammadzadeh, “Qubit mapping of one-way quantum computation patterns onto 2d nearest-neighbor architectures,” *Quantum Inf.Process.* **18**, 56 (2019).
- [75] F. Orts, E. Filatovas, G. Ortega, J.F. SanJuan-Estrada, and E.M. Garzón, “Improving the number of t gates and their spread in integer multipliers on quantum computing,” *Phys. Rev. A* **107**, 042621 (2023).
- [76] Stefan H. Sack, Raimel A. Medina, Alexios A. Michailidis, Richard Kueng, and Maksym Serbyn, “Avoiding barren plateaus using classical shadows,” *PRX Quantum* **3**, 020365 (2022).
- [77] Lucas Friedrich and Jonas Maziero, “Avoiding barren plateaus with classical deep neural networks,” *Phys. Rev. A* **106**, 042433 (2022).
- [78] Antonio A. Mele, Glen B. Mbeng, Giuseppe E. Santoro, Mario Collura, and Pietro Torta, “Avoiding barren plateaus via transferability of smooth solutions in a Hamiltonian Variational Ansatz,” *Phys. Rev. A* **106**, L060401 (2022).
- [79] Andrea Skolik, Jarrod R. McClean, Masoud Mohseni, Patrick van der Smagt, and Martin Leib, “Layer-wise learning for quantum neural networks,” *Quantum Mach.Intell.* **3**, 1–11 (2021).
- [80] Henry Eyring, “The activated complex in chemical reactions,” *J. Chem. Phys.* **3**, 107–115 (1935).
- [81] Matthew P. A. Fisher, Peter B. Weichman, G. Grinstein, and Daniel S. Fisher, “Boson localization and the superfluid-insulator transition,” *Phys. Rev. B* **40**, 546 (1989).
- [82] Xin-Yu Huang, Lang Yu, Xu Lu, Yin Yang, De-Sheng Li, Chun-Wang Wu, Wei Wu, and Ping-Xing Chen, “Qubitization of Bosons,” *arXiv preprint arXiv:2105.12563* (2021).

A. CIRCUITS OF PROBLEM-SPECIFIC ANSATZES

For completeness, we illustrate the HVA and HSA circuits for HM in Eq. (1) and TFIM in Eq. (7).

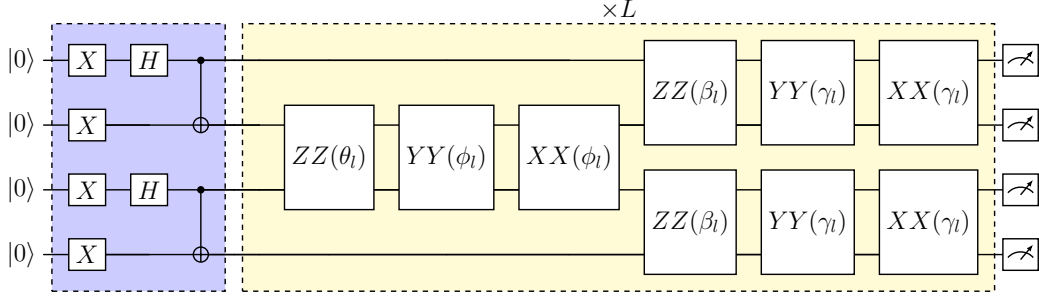


FIG. 19. The HVA circuit for HM in Eq. (1). In HVA, the parameters of the entanglers are correlated.

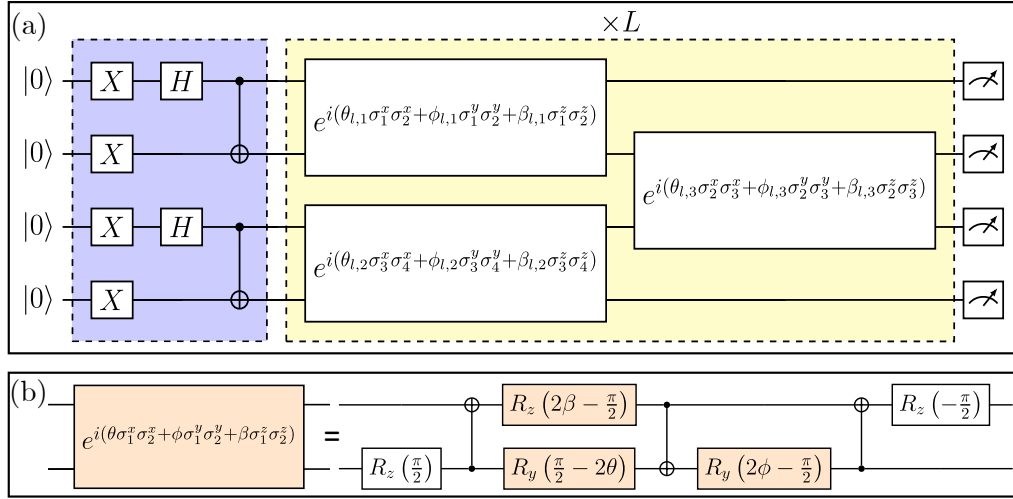


FIG. 20. The HSA circuit for HM in Eq. (1). (a) The architecture of HSA. (b) Circuit for realizing the entangler $e^{i(\theta\sigma_1^x\sigma_2^x + \phi\sigma_1^y\sigma_2^y + \beta\sigma_1^z\sigma_2^z)}$ used in HSA.

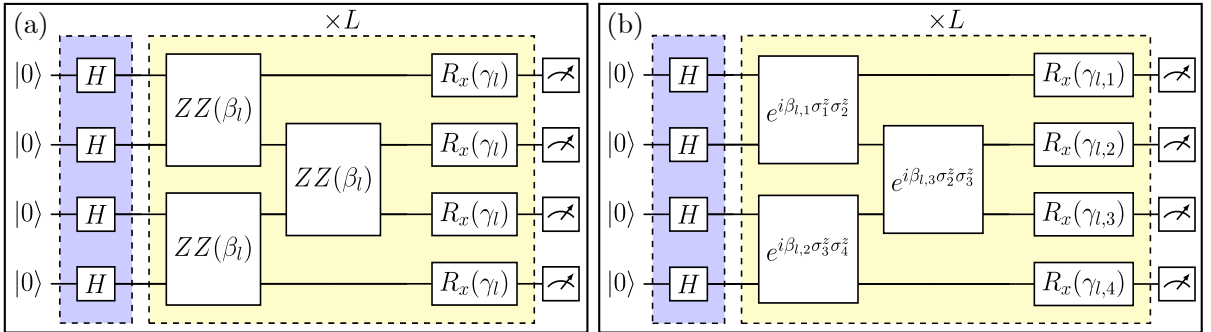


FIG. 21. The HVA and HSA circuits for TFIM in Eq. (7). (a) The HVA circuit. In each block, there are only two variational parameters, one for the single qubit rotational gates and the other for the entanglers. (b) The HSA circuit. The gates have different parameters in general. The entangler $e^{i\beta\sigma_1^x\sigma_2^x}$ can be realized by setting $\theta = 0$ and $\phi = 0$ in Fig. 20(b).

B. LIMITED MEASUREMENT SHOTS

We consider the practical case where the measurement shots are limited when evaluating the expectation of the Hamiltonian with respect to the output states of the circuits. We take the TFIM in Eq. (9) as an illustration. Here, we only compare the performance of three typical ansatzes: CZ-complete, HSA and our EHA. The experimental settings are the same as those in Fig. 5, except for the number of measurement shots. For the ideal case in Fig. 5, the shots are essentially infinite. Here, we consider three different numbers of shots to evaluate the expectation of the Hamiltonian, namely, 100, 1000 and 5000. The experimental results are demonstrated in Fig. 22. It is clear that our EHA outperforms HSA and CZ-complete.

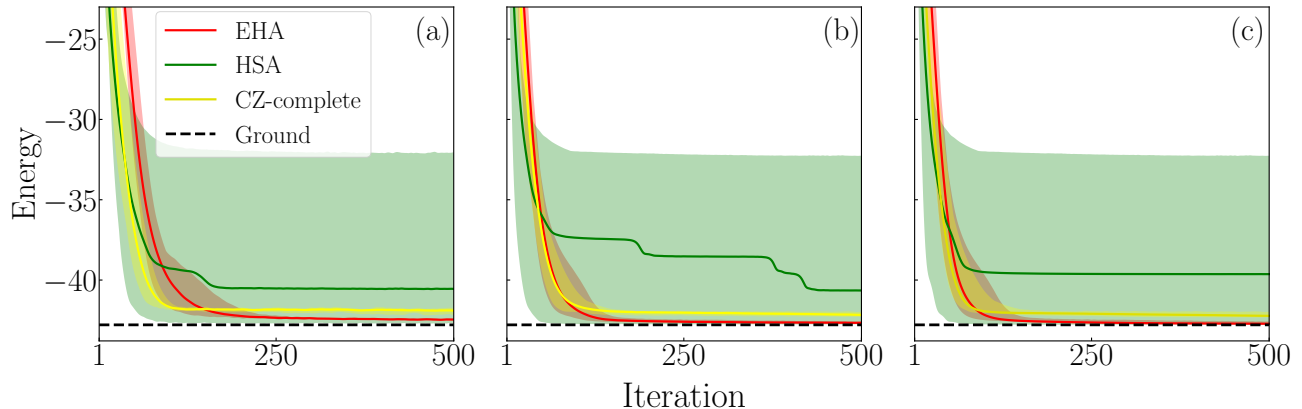


FIG. 22. Performance of EHA, HSA and CZ-complete under different numbers of measurement shots for the TFIM in Eq. (9). (a) Number of shots is 100. (b) Number of shots is 1000. (c) Number of shots is 5000.

C. RESOURCES FOR CHEMICALLY INSPIRED ANSATZES

Ansatz	Molecule	All CX gates	Non-local CX gates	T gates
UCCSD	H ₃ ⁺ (1.1)	272	32	0
UCCSD	HF(1.1)	2400	320	0
GRSD	H ₃ ⁺ (1.1)	64	45	16
GRSD	HF(1.1)	370	272	40
ADAPT-VQE	H ₅ (*)	306	246	24
ADAPT-VQE	BeH ₂ (1.1)	446	342	24
ADAPT-VQE	LiH(1.11)	366	283	32
ADAPT-VQE	HF(1.1)	152	109	24

TABLE IV. Resources for different chemically inspired ansatzes.

Here, for the H₅ molecule, (*) represents all bond lengths ranging from 0.5 to 1.5 with a step size of 0.1 (see Fig. 18).

D. THE IMPACT OF INITIAL REFERENCE STATES FOR HSA

From Fig. (23)(a), we find that for the HM, under the reference states $\otimes^{12}|+\rangle$ and $\otimes^{12}|0\rangle$, HSA cannot converge to the ground state. This validates that the performance of the problem-specific HSA is largely dependent on the reference state. This phenomenon can be explained by checking the corresponding entanglement transitions in Fig. (23)(b). We find that once the initial state is changed to $\otimes^{12}|+\rangle$ or $\otimes^{12}|0\rangle$, HSA cannot maintain the same amount of entanglement as the ground state, and in turn resulting in poor performance.

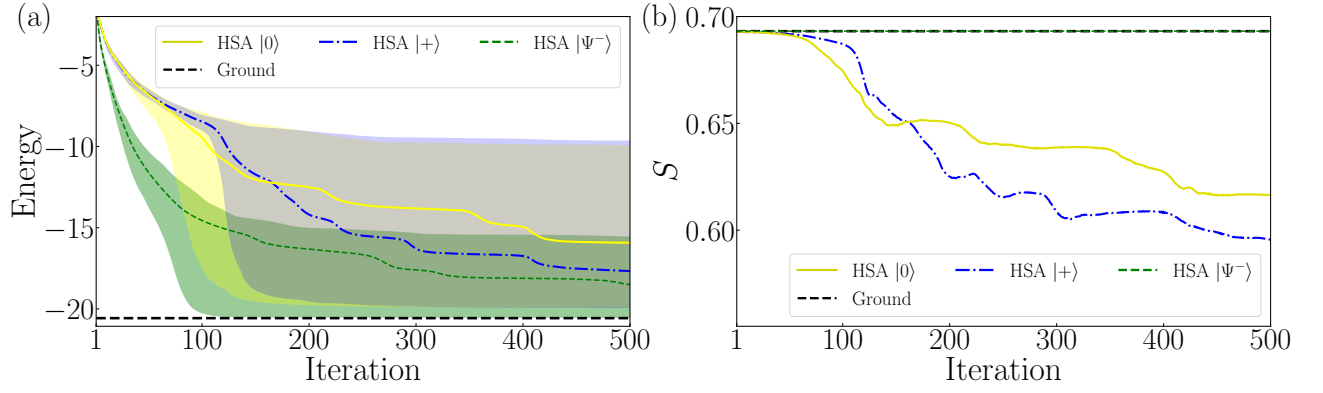


FIG. 23. Performance of HSA under different initial reference states for HM in Eq. (8). (a) The black dashed line denotes the actual ground state energy, and all the other lines indicate the respective average value of the energy over 10 realizations under different initial reference states. The shaded areas represent the smallest area that includes all the behaviors of the 10 realizations. (b) The black dashed line denotes the actual entanglement of the ground state, and all the other lines indicate the respective average value of the entanglement over 10 experiments under different reference states.

E. STEP SIZE SCHEDULE

Model	Step size	Iteration steps
BeH ₂ (1.1)	0.01	1000
	0.005	2000
LiH(1.11)	0.01	1000
	0.005	1000
HF(1.1)	0.01	1000
HM(8)	0.01	1000
HM(12)	0.005	1000
	0.001	1000
	0.0005	2000
HM(16)	0.005	3000
	0.001	2000
	0.0005	2000
TFIM1(8)	0.01	2000
TFIM1(12)	0.01	4000
TFIM1(16)	0.01	4000
TFIM2(8)	0.05	500
	0.02	1000
TFIM2(12)	0.02	1500
	0.01	2000
TFIM2(16)	0.02	1000
	0.01	4000
BHM(8)	0.01	1000
BHM(16)	0.01	500
	0.005	500

TABLE V. The step size schedule for different models.